



PERGAMON

Deep-Sea Research I 49 (2002) 1363–1386

DEEP-SEA RESEARCH
PART I

www.elsevier.com/locate/dsr

Multivariate objective analysis of the coastal circulation of Barbados, West Indies: implication for larval transport

Claire B. Paris^{a,*}, Robert K. Cowen^a, Kamazima M.M. Lwiza^b,
Dong-Ping Wang^b, Donald B. Olson^a

^a *Rosenstiel School of Marine and Atmospheric Science, University of Miami, 4600 Rickenbacker Causeway, Miami, FL 33149-1098, USA*

^b *Marine Sciences Research Center, State University of New York, Stony Brook, NY 11794-5000, USA*

Received 1 May 2001; received in revised form 30 December 2001; accepted 1 May 2002

Abstract

A multivariate spatial objective analysis (MVOA) assimilating high spatio-temporal resolution of hydrographic (CTD) and acoustic (ADCP) observations near Barbados provided a comprehensive view of the local surface circulation (0–100 m) during early spring of two consecutive years (1996 and 1997). Significant submesoscale fluctuations of the velocity and salinity fields exhibit a very dynamic environment. In the middle of each cruise, low-salinity water originating from the Amazon and entrained by a North Brazil Current Ring (NBCR) intruded from offshore and persisted on the west coast of Barbados throughout the rest of the survey. Principal component analysis (PCA) of velocity relative to the vertical structure and temporal factors in the study area demonstrated that the local circulation was mostly baroclinic and was dominated by a strong salinity front impinging on the island and large amplitude current reversals with a periodicity of ca. 20 d. During transition times, indicated by a change of the sign of the amplitude of the empirical orthogonal function (EOF), the flow became barotropic. This situation produced strong southward currents followed by the onset of vertical velocity shear. Most of the flow variability occurred in the upper 40 m of the water column, which was also found to be the depth of penetration of the low-salinity lenses. These results indicate that the NBCR structure was retained during both intrusions. Lagrangian trajectories using the MVOA currents were found to be consistent with in situ drifter trajectories, suggesting that the analyzed flow field is representative of the near-shore circulation. Tracking of particles released in the surface layer (0–20 m) from the reef shows a maximum residence time of 18 d indicating the possibility of larval retention within the island-scale flow field. Finally, our results suggest that MVOA, within its limitations, is a powerful tool that can be applied elsewhere to infer circulation and larval transport, even in situations when forcing is unknown. © 2002 Published by Elsevier Science Ltd.

Keywords: Spatial objective analysis; Current data; Larval fish transport; North Brazil Current Ring; Caribbean Island

1. Introduction

At low latitudes, where oceanic waters tend to be oligotrophic, the coastal environment of islands is key in maintaining marine populations, in particular, because it represents both an important

*Corresponding author.

E-mail address: cparis@rsmas.miami.edu (C.B. Paris).

source of nutrients for the pelagic early life history stages and diverse habitat for the adults. Possible accumulation of the larvae and the existence of stable or predictable conditions within the high-energy, complex near-shore environment are major factors leading to retention of larvae of coastal species near suitable habitat for recruitment. In contrast, processes favoring diffusion, mixing, or unstable events may lead to dispersal and loss of larvae from local populations. Temporal and spatial variability of the coastal environment translated into transport and nutrient variability may play a determinant role in the survival of larvae (Richards, 1982). To accurately define and predict larval transport, it is essential to quantify the time/space scales of the complex coastal current features that promote retention or dispersal (Okubo, 1994). In addition to tidal, wind and buoyancy forces, coastal currents have a strong spatial dependence due to bathymetric constraints. Interference of geostrophic jets with the topography brings inertial instabilities (Smith and Schwing, 1991), and the resulting circulation patterns are usually dynamic on a broad range of spatial and temporal scales (Haidvogel et al., 2000). Scale variability of coastal circulation dynamics may increase for island environments where an island is embedded in a complex incident flow. Island-mass effects (Boden, 1952; Chopra, 1973; Hogg et al., 1978; Sanders, 1981), eddies on the down-current side of islands (Boehlert et al., 1992), and currents steered by local topography (e.g., steepness of the bottom slope) inducing friction (Hogg, 1972, 1980; Cowen and Castro, 1994) all represent additional processes that render island circulation even more complex. Previous studies of island circulation have described general flow patterns based on hydrographic properties, satellite-derived sea level anomalies, and wind forcing (Bowman et al., 1994; Chiswell and Booth, 1999; Polovina et al., 1999). Only a few studies based on modeling (Rosenfeld et al., 1989; Liu et al., 1999; Simmons and Nof, 2000) and remote sensing (Barton et al., 2000) have focused on assessing the importance of external forcing on the local circulation. Yet, they have not quantified the temporal variability of the flow and its response to variable forcing at the island-scale, which is also

critical to resolving larval transport. Description of the near-shore dynamics in the vicinity of an island requires a high-resolution sampling scheme, in both time and space, combined with highly optimized analytical methods.

In this study, the oceanic island of Barbados was selected for its isolated location on the eastern flank of the Lesser Antilles, minimizing the likelihood of larval input from upstream sources, and its extremely dynamic environment. Barbados lies in the path of the Guyana Current and is downstream of many of the rings shed by the North Brazil Current (NBC; Fratantoni et al., 1995; Goni and Johns, 2001). The dynamics of the island-scale flow at Barbados is driven by the variable nature of the incident flow interacting with the local topography (Bowman et al., 1994). Several areas of larval concentration were previously identified that were clearly coupled with persistent local flow features (Cowen and Castro, 1994). One of these concentration areas was located off the western shore of the island, where a slow, onshore flow was found in the subsurface layer below the upper 25 m. Two exceptional physical flow events were identified as strong current reversals and surface salinity fronts, each representing a potentially large source of variation in the recruitment of reef fishes to Barbados (S. Sponaugle, unpublished data). The flow events are consistent with rings generated by the NBC retroflection, which translate northwestward in the Guyana Current to the Lesser Antilles (Johns et al., 1990; Richardson et al., 1994; Fratantoni et al., 1995), although salinity fronts may not always be concurrent to NBC Rings (NBCRs) (Flagg et al., 1986). Stansfield et al. (1995) demonstrated that during the passage of a shallow low-salinity pool south of Barbados, strong unidirectional currents replaced the weak and variable coastal currents. Analysis of satellite (TOPEX) and of temperature–salinity recorders moored off the west coast of Barbados by Kelly et al. (2000) revealed that NBCRs pass Barbados more frequently than previously thought (Fratantoni et al., 1995), bringing pools of low-salinity water from the Amazon. Clearly, these low-salinity intrusions interfere with the already variable island-scale flow around Barbados. These previous reports have described the NBCR as a

distinct mesoscale process influencing the island circulation, but there is a need for quantitative assessment of the effects on the temporal and spatial variability of the near-shore flow structure. Knowledge of the magnitude and the scales of variability of coastal current dynamics is of paramount importance for the study of reef fish recruitment, since the near-shore environment modulates the transport of locally hatched larvae by enhancing either dispersal or retention.

The primary objective of this study is to provide a description of the near-shore surface circulation patterns off Barbados and establish a link between the local circulation and the low-salinity events identified from previous larger scale surveys around the island (Cowen and Castro, 1994) and from a concurrently deployed ADCP mooring. The secondary objective is to produce a time series of 3-D velocity fields to identify major flow structures, quantify the temporal and spatial scales associated with the flow dynamics, and infer larval transport. A specific goal is to provide high-resolution spatial and temporal measurements of the flow regime operating at the same scales as ichthyoplankton processes, which will serve ultimately in assessing biophysical interactions involved in larval transport.

In this paper, first we present an analytical model of the circulation, based on a multivariate objective analysis (MVOA) originally described by Pedder (1989) for atmospheric data and further applied to oceanography by Pinot et al. (1995a) and Gomis et al. (2001). The MVOA generates for each year of the study a time series of horizontal currents at various depth levels, which give a comprehensive view of the 3-D coastal circulation. Second, the MVOA flow field maps are quantitatively analyzed by PCA, a technique that we are using (1) to verify that the maps of horizontal currents provided by MVOA are vertically and temporally coherent and (2) to determine the dominant patterns of the local circulation at various time and space scales (Mariano et al., 1996; Larson et al. 1999). Finally, the resulting velocity field is used to infer Lagrangian characteristics of the flow, with the future intent of modeling larval transport on the western shore of Barbados.

2. Methods

2.1. Field sampling scheme

The research presented here is part of a larger interdisciplinary project investigating the physical processes affecting the dispersal and survival of the pelagic phase of locally spawned coral reef fishes. To minimize the likelihood of external sources of larvae, the study took place off the isolated oceanic island of Barbados ($13^{\circ}10'N$, $59^{\circ}30'W$), West Indies. It consisted of two 30-d cruises on the R./V. *Seward Johnson* during May–June of two consecutive years, 1996–1997. Based on our previous finding of the highest larval densities along the western shore of Barbados (Cowen and Castro, 1994), the study region was limited to an area extending 15 km from the west coast and 25 km parallel to shore (Fig. 1). Sampling involved repeated 3-d physical and biological surveys. During day 1, a conductivity-temperature-depth (CTD) survey was conducted with a Sea-Bird SBE9 in a grid pattern covering the domain to provide a quasi-synoptic temperature/salinity field. CTD transects ran parallel to shore and were spaced about 3 km apart within the sampling area and, on average, 21 CTD casts (ca. 4 km apart) were taken to a maximum depth of 500 m or to within 25 m from the bottom. To maximize sampling resolution, Acoustic Doppler Current Profiler (ADCP) data were continuously recorded along the ship track with short-term maximum error estimates on bottom-tracked velocity of 6 cm s^{-1} at 400 m. The ADCP data was acquired at a vertical resolution of 4 m and 300 s sampling ensembles. During day 2, 24 vertically discrete ichthyoplankton samples at 20-m intervals from the sea surface to 100 m were taken in a 12-h day/12-h night paired sampling, also concurrent with ADCP profiles. The biological data will be presented elsewhere. Finally, during day 3, 4–8 ARGOS/GPS tracked drifters were deployed within the study domain and retrieved at the end of the 24-h period. To capture both the surface layer and lower layer flow, half of the drifters were drogued at 10 m and the other half were drogued between 40 and 70 m depth. This 3-D sequence was repeated a total of eight times (surveys) during the

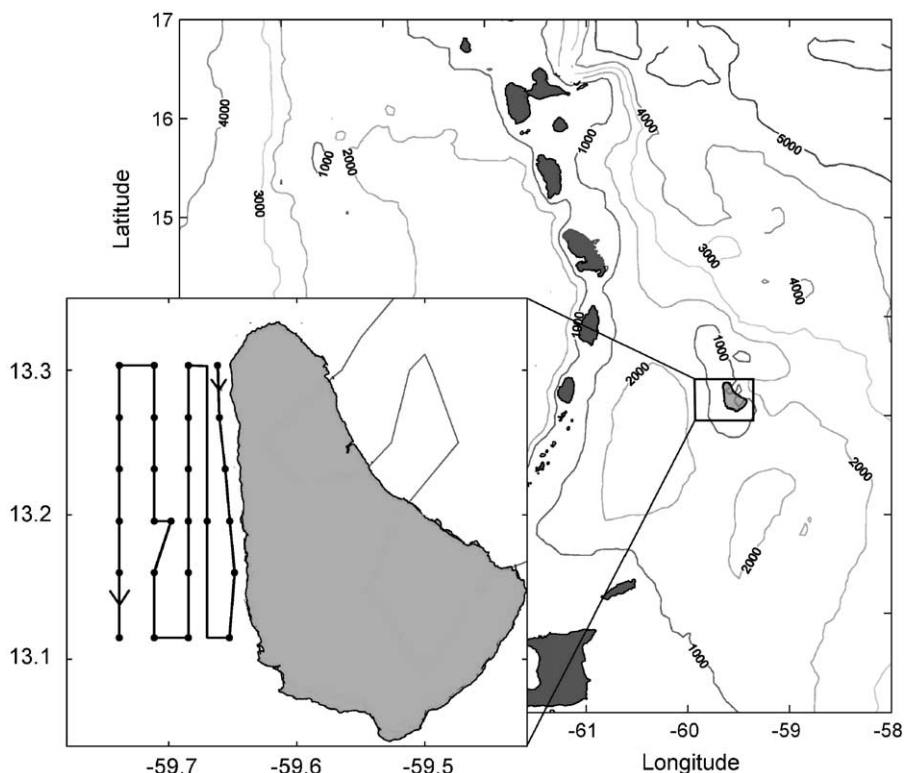


Fig. 1. Sampling scheme at Barbados, West Indies: CTD stations and ADCP ship track, for each 24-h sampling period (survey).

cruise. The entire experiment was repeated during the following year.

2.2. Flow field model

MVOA was used to obtain a series of horizontal fields of total velocities at various levels by assimilation of CTD and ADCP data sampled by scattered profiles. This method, described by Gomis et al. (2001), improves the diagnosis of currents by (1) minimizing the variance between observation points and (2) reproducing the dynamic (geostrophic) balance between the variables. The space distribution and the quasi-synoptic nature of the CTD and ADCP sampling of our study permitted the use of this optimal statistical method. An advantage of MVOA is that it generates outputs of total velocities partitioned into non-divergent and irrotational components, thereby allowing the evaluation of the ageos-

trophic component of the velocity field. In addition, this process of estimating velocity values in a field is reproducible at any location without the need of any explicit specification of external boundary conditions. The two variables that were used in the optimum interpolation were dynamic height and flow fields retrieved from the sampling as follows.

2.2.1. CTD data analysis

Assuming that the 24-h CTD observations were quasi-synoptic, dynamic heights were computed for each CTD survey (Pond and Picard, 1983) with the MATLAB program file SEAWATER/sw_gpan.m ©. The reference level, which represents an important assumption for the validity of the resulting current field in the MVOA (Gomis et al., 2001), was set to 200 m since horizontal variability of dynamic height relative to the sea surface was negligible below this depth (maximum

dynamic height difference of 0.35 dyn cm at 200 m). For the most near-shore CTD transect, this level of reference intersected the bottom. The ‘missing’ water column (from the bottom to 200 m) at each station was replaced by the closest station on the next CTD transect. This assumed that the component of the geostrophic velocity below the shallow stations depth, normal to the line between the two stations involved, was negligible (Pinot et al., 1995a). Distribution of dynamic height at the surface is shown for one survey in Fig. 2a. Because the forcing of the flow is unknown, it is important to have independent observations of velocities, besides dynamic heights. ADCP data are a good candidate for that, since measurements are very reliable on the continental margin (<400 m).

2.2.2. ADCP data analysis

To produce a homogeneous ADCP data array required in MVOA, bottom-tracking ADCP data obtained for depths <400 m were processed as follows. First, to remove erroneous velocities, all data were filtered by elimination of velocity values greater than the mean + 1.96 standard deviation (corresponding to 95% of the normalized values around the mean; Sokal and Rohlf, 1995). Second, the on-station data that produced a tight cluster of vectors (Fig. 2b) were spatially averaged within 150 m of each station and a single profile was returned for approximately each 3-km segment of underway data for every five profiles on the ship track (or an average of 50 ADCP profiles per survey).

2.2.3. Multivariate scheme for Barbados

The ADCP and CTD data processed as described above were analyzed from the surface to 100 m on 5 horizontal planes (every 20 m) and returned velocities in a 12×12 mesh, corresponding to a $2.2 \text{ km} \times 1.1 \text{ km}$ grid (Fig. 2c). The maximum depth for the flow field output corresponds to the depth limit of ichthyoplankton sampling, which also approximates the depth of the inshore CTD line. The mesh size was determined by the density of observed data and is a compromise between increasing precision and minimizing error. A characteristic scale factor (L_s) was used in the MVOA to eliminate smaller scales that cannot be resolved by the sampling (i.e. CTD

station separation of 2–5 km). In the context of a 24-h survey, the shorter structures (< L_s) are considered transient features that are misrepresented by the time and space scales in the sampling, such as inertial motions. Based on these considerations, L_s was set up to 7 km, which corresponded to the smallest resolvable feature or about twice the spacing of input data (e.g. distance between stations; Gomis et al., 2001). This choice of characteristic length scale also resolved the horizontal scale of the current structure revealed by the auto-correlation function of the meridional velocity component; this scale ranged from 5 to 8 km. Since the ADCP measures the total current, it includes ageostrophic flows such as wind-driven current, tides, and near-inertial motion. Tides in Barbados are semi-diurnal, with ca. 10 cm s^{-1} amplitude (estimated from the ADCP mooring, cf. Kelly et al., 2000), and were not explicitly removed from the total current. The ADCP data had greater spatial resolution than the CTD data (input includes 45–55 ADCP and 16–24 dynamic height observations), consequently MVOA is weighted towards the ADCP data, and dynamic height contributes to the analysis only when it is consistent with the velocity data.

A sensitivity analysis was performed in multiple steps to separately assess the contribution of different data sets to the final flow field output. First, only ADCP data were entered into the OA scheme (univariate analysis), and the resulting non-divergent flow field was quantified. Second, only CTD data were entered to establish a geostrophic circulation. There was good agreement between the ADCP flow field at the surface (10 m level) and the CTD stream functions. Therefore, the correlation parameter between geostrophic stream function and non-divergent stream-function, which is usually within the range 0.9–1.0 in the ocean (Pinot et al., 1995a), was set at 0.95 for the MVOA scheme utilizing both ADCP and CTD data. An additional parameter required in MVOA is the noise-to-signal ratio, which serves to determine the extent to which dynamic height and total current estimates can deviate from observations (i.e. observational error). This ratio was set to 0.1 for both the geostrophic stream function and the velocity observations, resulting in

of larger scales was to increase the smoothing of gradients, although the pattern of circulation was not really modified. The choice of 7 km was maintained since the resulting dynamic height field agreed well with the observed dynamic height gradient (Fig. 2c).

Following the above scheme, dynamic heights and observed ship ADCP velocities integrated over 20-m layers were assimilated into the MVOA to generate 3-D horizontal velocity fields for each survey (Fig. 2d). This technique removed noise from scattered sampling and produced self-consistent maps of the horizontal total current in the coastal waters of Barbados.

2.2.4. Principal component analysis (PCA)

The velocity data resulting from the MVOA were analyzed by means of PCA, a technique used to determine variability and dominant patterns of oceanographic factors at various time and space scales (Mariano et al., 1996; Pedder and Gomis, 1998; Larson et al. 1999). The principal objectives of this quantitative analysis were (1) to verify whether the flow fields are temporally and spatially coherent since each 20-m layer was obtained independently, and (2) to identify and quantify the dominant circulation variability patterns of the island-scale circulation.

PCA on the velocity data was performed relative to the surveys and to the layers, including all grid points. The depth interval (0–100 m) of the PCA was limited by the five 20-m layers of the MVOA maps (note that the data are specified for $l = 5$ depth-layers referred as levels, and $n = 8$ surveys). The variables for the PCA were taken from the (x, y, z) coordinates of the MVOA velocity maps, having the dimensions of $(12 \times 12 \times 5)$, or 720 values per survey, and a total of 5760 points per cruise. Principal components (PCs) were calculated in both horizontal and vertical mode decomposition. First, least squares were fitted over n for each (x, y, n) , where the n temporal eigenvectors represented the set of independent variables. Second, the fit is carried out over l for each (x, y, l) , such as l vertical eigenvectors represented the independent regression variables. The resulting regression coefficients are the PC amplitudes for each significant temporal/vertical

eigenvector. The results of the PCA are visualized through time series of modes amplitude and PCs variance, vertical profiles of the PC amplitudes for the first two statistical modes, and spatial maps of the first mode EOFs.

2.2.5. Lagrangian integration

To establish trajectories and their associated time scales, Lagrangian integration was performed on the optimum interpolated velocities. The MVOA velocities were interpolated stepwise (every 6-h) between each survey, producing a continuous flow field. A turbulent field produced through a random-flight scheme was superimposed on the deterministic velocity field to predict diffusion (Thompson, 1986). At constant time steps ($dt = 60$ s), a turbulent component of the velocity moves the particle an extra displacement from the deterministic displacement ($dt = 6$ s). In addition, the evolution of the turbulent velocity $u(t)$ is assumed to be a Markov process by which each time the particle moves through the flow field, it loses a fraction of its momentum to the surrounding fluid and in turn receives a random impulse from a Gaussian random number generator (Dutkiewicz et al., 1993). Although this implies discontinuous acceleration of particles, it is more realistic than a Markov process on the particle displacement $x(t)$ that would imply a discontinuity in the velocity field. The diffusion coefficient ($K = 2 \times 10^4 \text{ cm}^2 \text{ s}^{-1}$) resulting from the imposed stochastic movement was adjusted to match the horizontal eddy diffusivity characteristic of the spatial scales prescribed by the grid size ($1.1 \text{ km} \times 2.2 \text{ km}$; Okubo, 1971). Qualitative validation of this transport model was performed by comparing real drifter trajectories with those of particles released at the same time and location. To simulate fish spawning along the reef track, patches of 1000 particles were released at each cell of the 11th column of the 12×12 grid in the surface (layer 1: 0–20 m). Because hatching does not occur instantaneously in most reef fish species, the 1000 particles were released progressively during a 24-h period. Spawning was simulated for a series of 12 consecutive days, starting on day 1 of the survey. Retention was calculated on a daily basis as the percent of particles remaining in the domain.

3. Results

3.1. Hydrography (CTD data)

During the first four surveys in both 1996 and 1997, the surface salinity was greater than 35 units throughout the upper 100 m (Fig. 3a and b). In both years, a strong low-salinity front appeared from offshore in survey 5, separating salty coastal

water from fresh and slightly warmer oceanic waters. This front moved rapidly over the entire domain, which remained lower in salinity for the next three surveys. When the salinity front penetrated the domain in both years, the stratification intensified and was first associated with downward isohalines towards the coast (survey 5), then with upward sloping (Fig. 4a and b). In

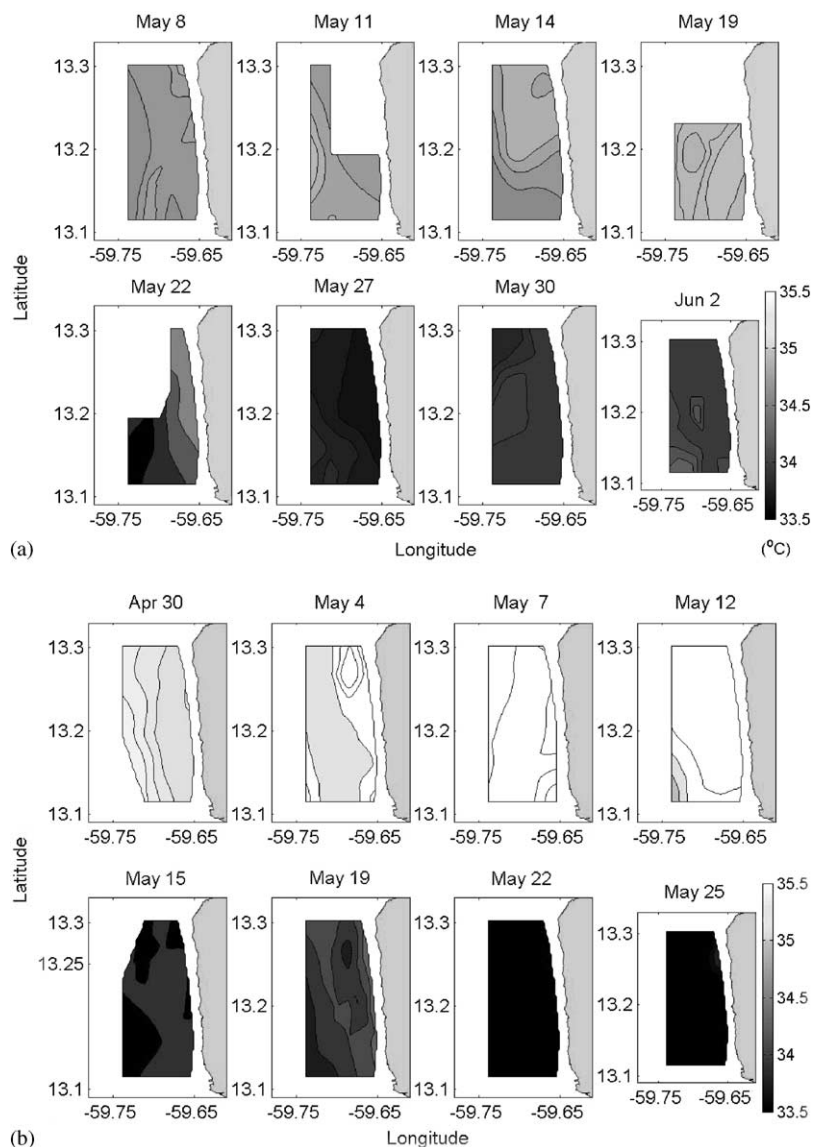


Fig. 3. Horizontal distribution of salinity (a, b) and temperature (c, d) from CTD observations at 3 m and per sampling period in 1996 (a, c) and 1997 (b, d).

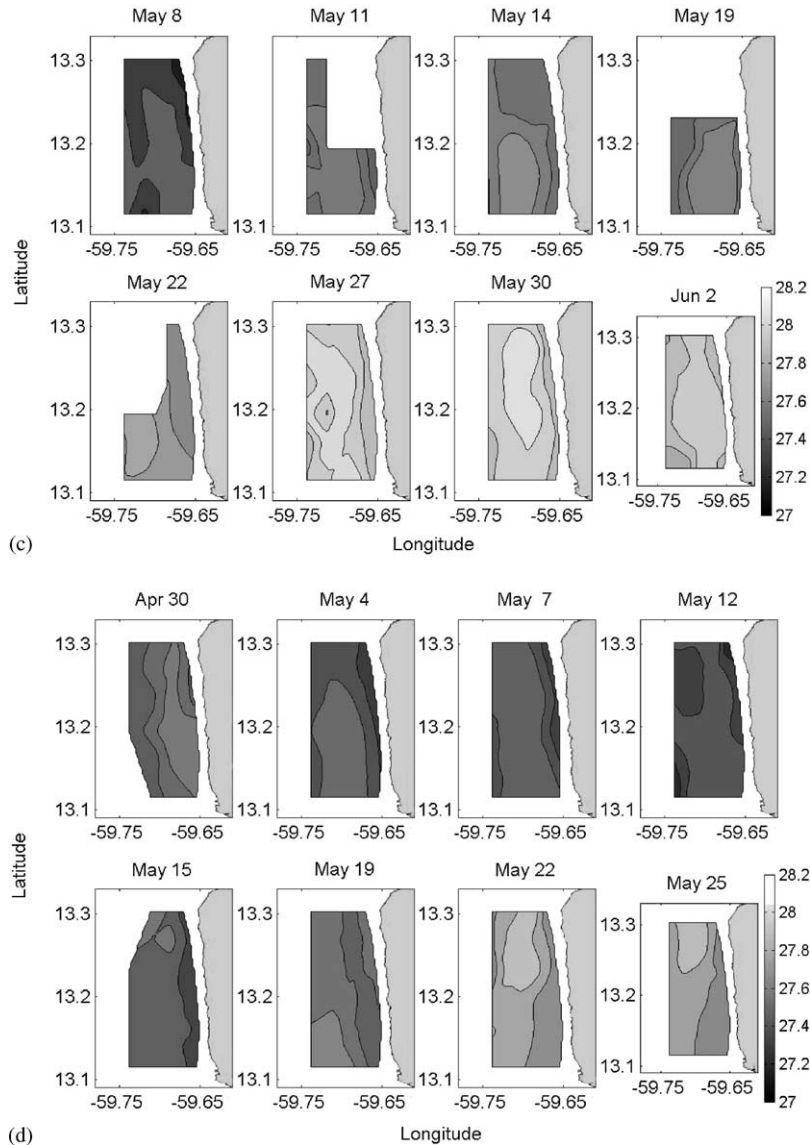


Fig. 3 (continued).

1996 the low-salinity front was coupled to warmer sea surface temperatures (Fig. 3c). However, in 1997, although the change in salinity was larger (> 2), warm waters near the surface lagged by two surveys (Fig. 3d).

3.2. Velocity (ADCP data)

In general, current velocities resulting from the ADCP data alone differed only slightly in direc-

tion and intensity (maximum difference of 6 cm s^{-1}) from those derived from the CTD data alone (univariate analysis). These differences are partly due to differences in high frequency limits of the CTD and ADCP fields (CTD sampling was less dense than the ADCP underway profiling), and partly to divergence in the flow represented by the ageostrophic and irrotational components (Fig. 5). Currents exhibited strong meridional and zonal velocities in the upper 20 m with

infrequent maxima of 80–110 and 50–90 cm s^{-1} , respectively (Fig. 6). The flow was temporally variable since the meridional component of the

velocity reversed in the upper 80–100 m three times during the 30-d sampling period each year (surveys 3, 5 and 7; Fig. 7) and exhibited maximum shear

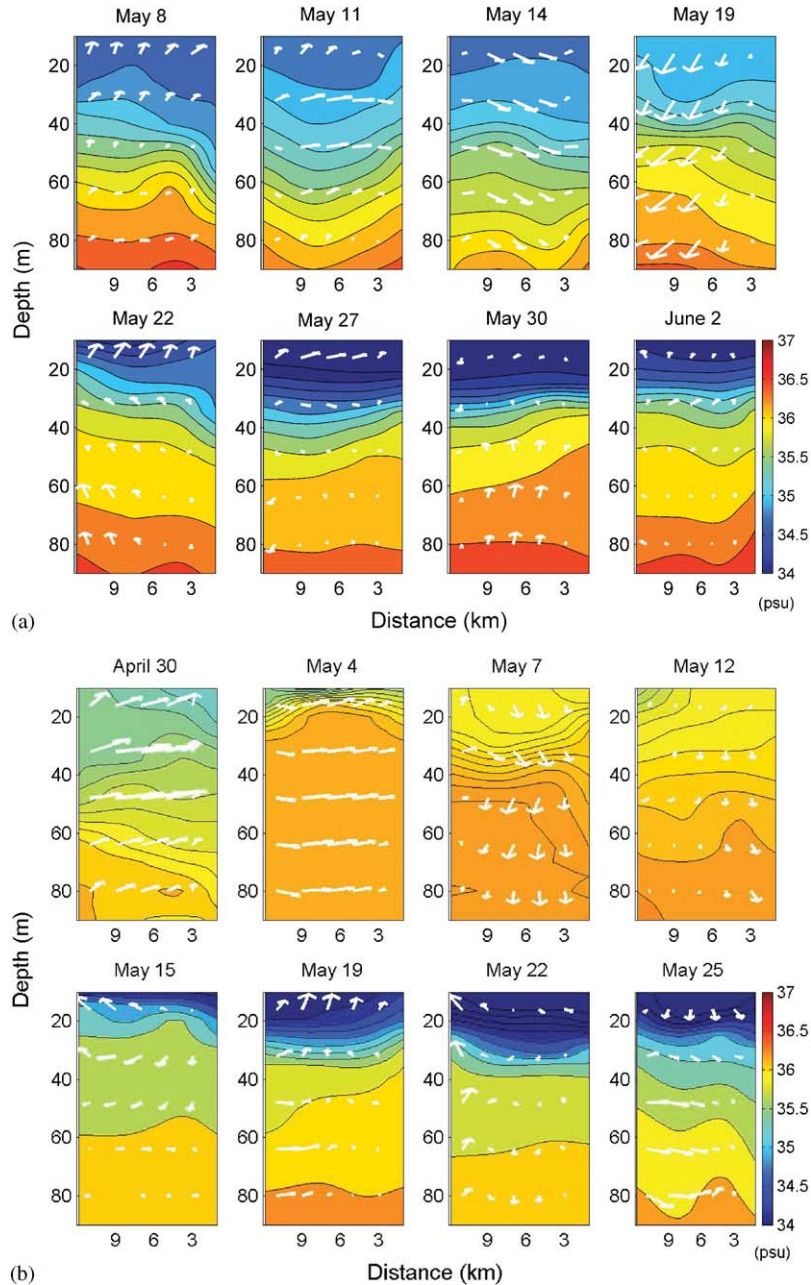


Fig. 4. Mean alongshore vertical salinity (a, b) and temperature (c, d) fields per sampling period in 1996 (a, c) and 1997 (b, d). Superimposed are the horizontal velocities obtained from the multivariate spatial analysis, where up is north and down is south; max velocity = 50 cm s^{-1} .

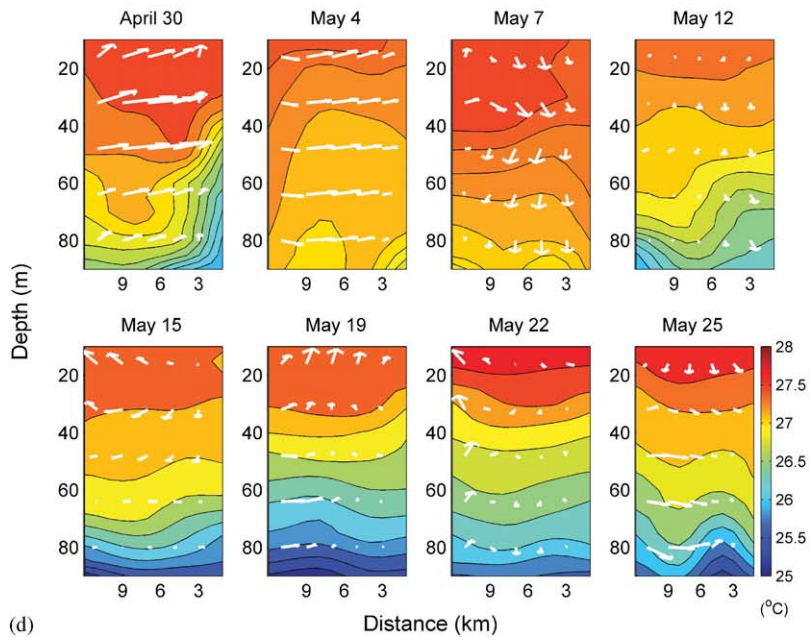
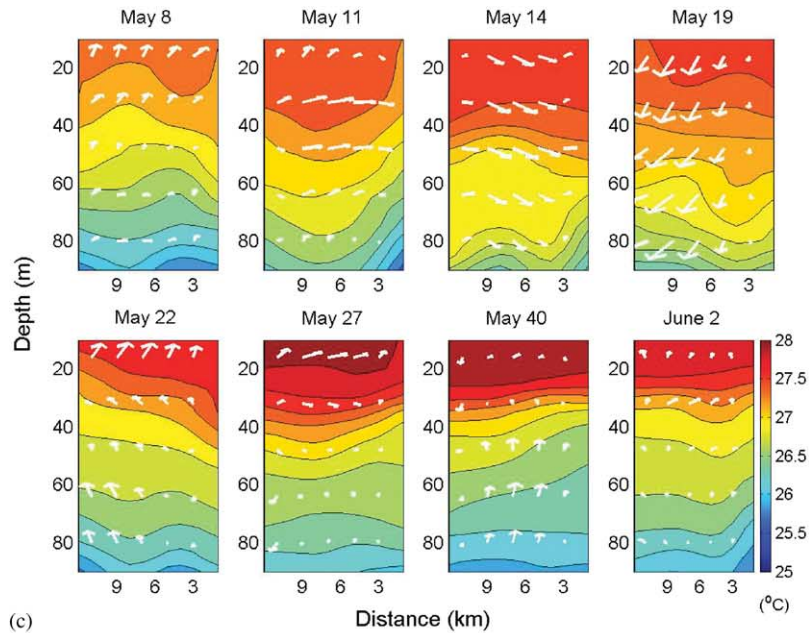


Fig. 4 (continued).

during those current reversals; the corresponding standard deviations were coherent for both velocity components. Surface circulation was intensified in the N–S, and, in general, there was a

subsurface maximum onshore flow, except during the intrusion of the low-salinity front, when the subsurface flow was offshore (survey 5 in both years).

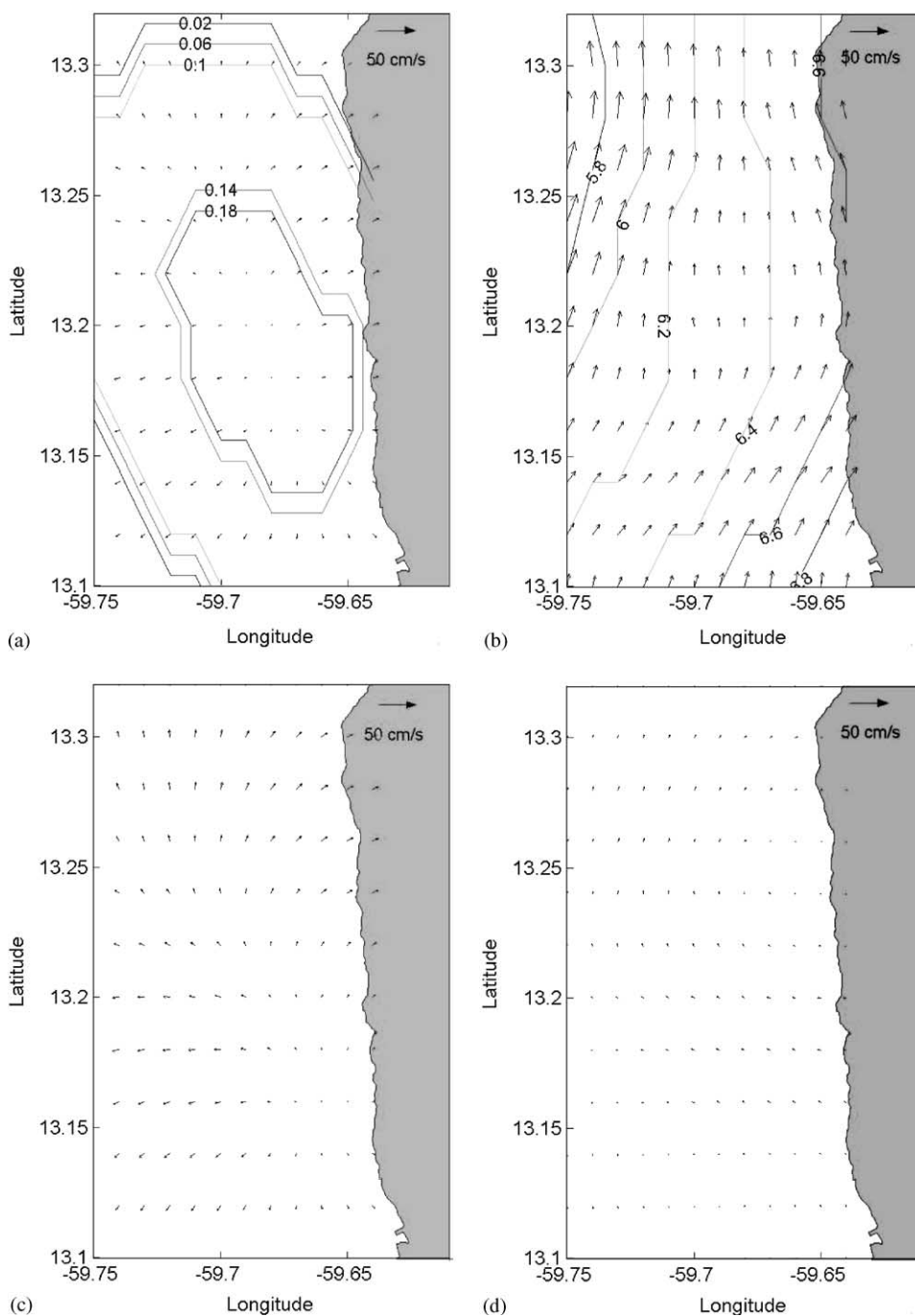


Fig. 5. Flow components produced by the multivariate analysis at the 10m level during the first survey of 1996 (reference level at 200 m): irrotational current and velocity potential (dyn cm) (a); non-divergent current and stream function (dyn cm) (b); ageostrophic current (total current minus geostrophic component) (c); non-divergent ageostrophic current (non-divergent current minus geostrophic component) (d).

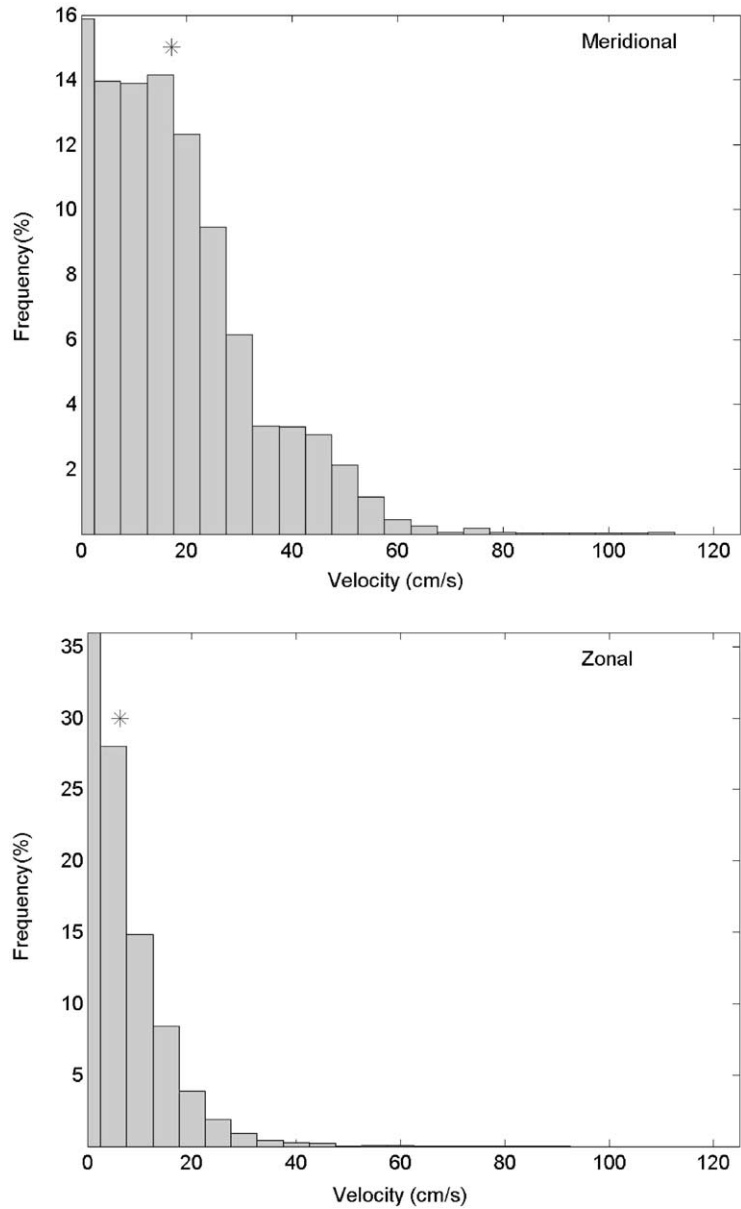


Fig. 6. Frequency distribution of meridional (a) and zonal (b) ADCP velocities from the surface bin (12 m) during May 8–June 2, 1996; asterisks indicate modal values.

3.3. Circulation (0–100 m)

Comparison of the dynamic height fields estimated by MVOA and those measured with CTD data shows that the MVOA procedure reproduced well the major features observed in the salinity/

temperature field. However, for both years there was disagreement between the geostrophic and total currents prior to the intrusion of low-salinity waters into the sampling area. This suggested that ageostrophic effects were important during those transition periods associated with changes in

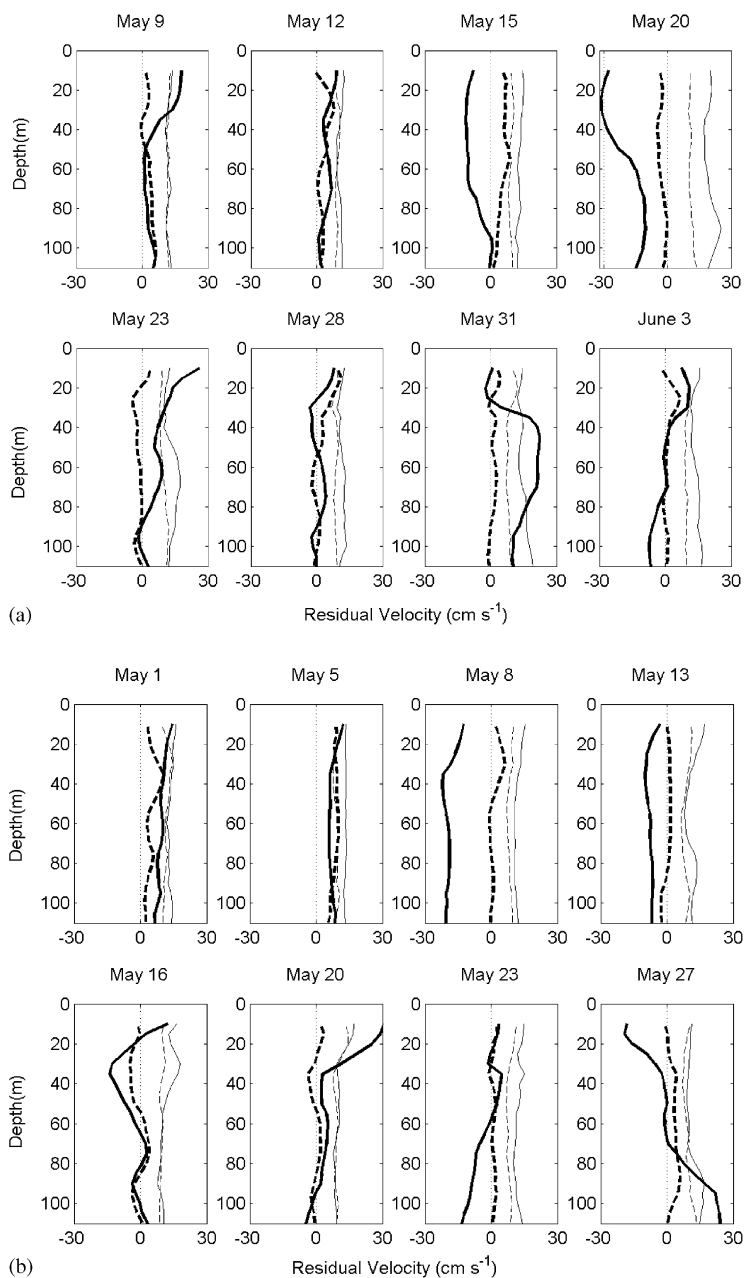


Fig. 7. Residual ADCP velocity profiles in the sampling domain and their positive standard deviation (thin lines) from 0 to 100 m per sampling period in 1996 (a) and 1997 (b); meridional velocities are solid lines, zonal are dashed lines.

density gradients. In the upper 100 m, the flow was consistently more dynamic in the surface layer (0–20 m) than in the deeper layers, where low flow regions were found and the cross-shelf horizontal

velocity fields showed that the flow was mostly baroclinic. Yet, preceding the low-salinity intrusion the current became barotropic and was flowing southward at velocities greater than 50 cm s^{-1}

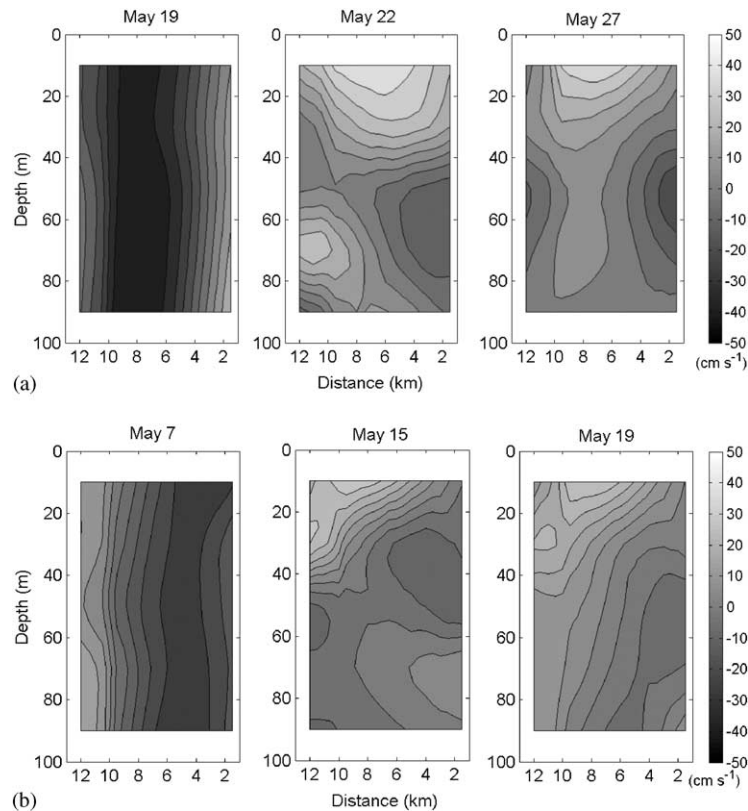


Fig. 8. Meridional MVOA velocity from a middle section of the sampling domain preceding and during the low-salinity intrusion for 1996 (a) and 1997 (b); velocity is contoured every 6 cm s^{-1} .

throughout all the 5 layers (Fig. 8). Subsequent penetration of the low-salinity lens in the domain was coupled with a maximum velocity shear in the 20–40 m strata, coinciding with the depth of the strong halocline formed during stratification.

3.4. Principal component analysis (PCA)

When PCA is performed separately for each survey for all grid points, the motion is found to be highly coherent in the vertical, as most of the variance is explained by the first two modes. Time series of the PC variance (Fig. 9) illustrates that for most of the surveys mode 1 was greater than mode 2, both explaining most of the variance (40–90%). This indicates that the MVOA flow is temporally coherent and mostly baroclinic, with surface intensification. The relative decrease in the variance explained by the first mode leading and

following the low-salinity intrusion corresponds to a relaxation from one regime to another and coincides with the strong flow reversals. Although the first mode peaked 6 d earlier in 1997, the general trends in PC variance are similar for both years, retaining the signature of a typical event (ca. 20 d cycle).

Since the circulation within each survey and throughout the entire study period appears quite coherent, PCA is now performed jointly on all surveys to examine the current fluctuations over the entire study period. Spatial and temporal scales of the dominant horizontal current features are obtained by plotting the eigenvectors from the dominant mode. For this purpose, we built the matrix of dimensions $N \times M$, where

- (1) $N = 8$ (dimension of survey= n) and $M = 12 + 12 + 5 + 2$ (dimensions of x , y , level (l),

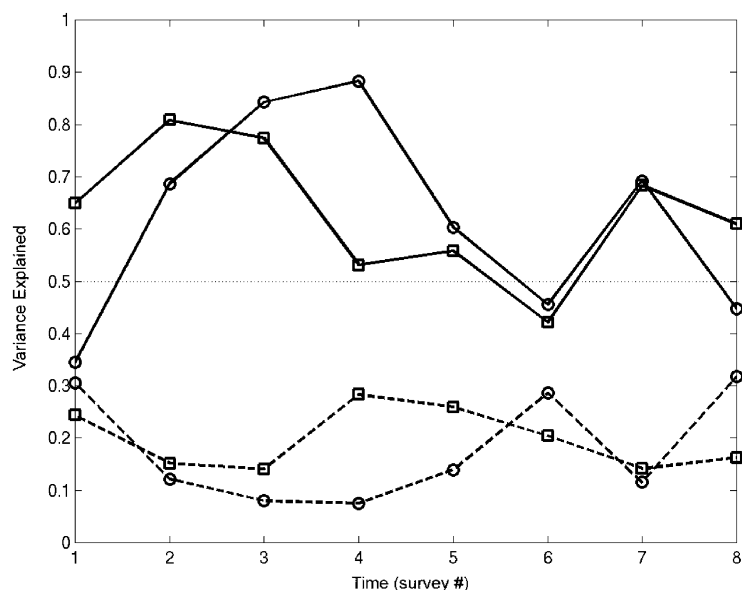


Fig. 9. Time series of the variance explained by the 1 (solid lines) and 2 (dotted lines) mode PCs in May of 1996 (circle) and of 1997 (square).

u , and v) for horizontal mode decomposition. The resulting mode 1 and 2 PCs give the amplitude time series over a month period (Fig. 10a). The first mode is indeed meaningful since it indicates that the current reverses during surveys 3, 5 and 7 in both years, corresponding to the observed current reversals (Fig. 7). The first EOFs generate velocity variability maps for each survey whereby a positive EOF implies values greater than the 5-layer mean, and vice versa (Fig. 10b and c). During the first four surveys, the variability in current direction is minor, compared to the rest of the month. The area of greatest variability is found in the northeast corner during survey 5 of 1996, where the saltier coastal waters are wedged by the salinity front coming from offshore. In 1997, the highest variability currents penetrate the domain through the southwest and move towards the northeast by survey 6.

- (2) $N = 5$ (dimension of level = l) and $M = 12 + 12 + 8 + 2$ (dimensions of x , y , survey (n), u , and v) for vertical mode decomposition. The resulting PC amplitudes are similar for both years where the first baroclinic mode is large

for the 2 uppermost layers (0–40 m), and flips sign in the 40–60 m layer (Fig. 11a). This indicates that the velocity variability increases towards the surface; the zero crossing between the 20–40 m and 40–60 m layers corresponds approximately to the depth of penetration of the low-salinity pools. The second baroclinic mode has a different structure, changing sign twice in the vertical for both cruises, with a subsurface maximum. This mode could correspond to the non-NBCR situation, when an onshore flow is found in the 20–40 m layer. The first EOFs generate the velocity variability maps for each 20-m layer, whereby a positive EOF implies values greater than the 30-d mean (Fig. 11b and c). As expected from previous findings of Cowen and Castro (1994), the dominant variability signal in the surface layers is a strong alongshore current, and at depth the dominant flow feature is onshore.

3.5. Lagrangian integration

Trajectories derived from Lagrangian integration were found to be consistent with in situ drifter

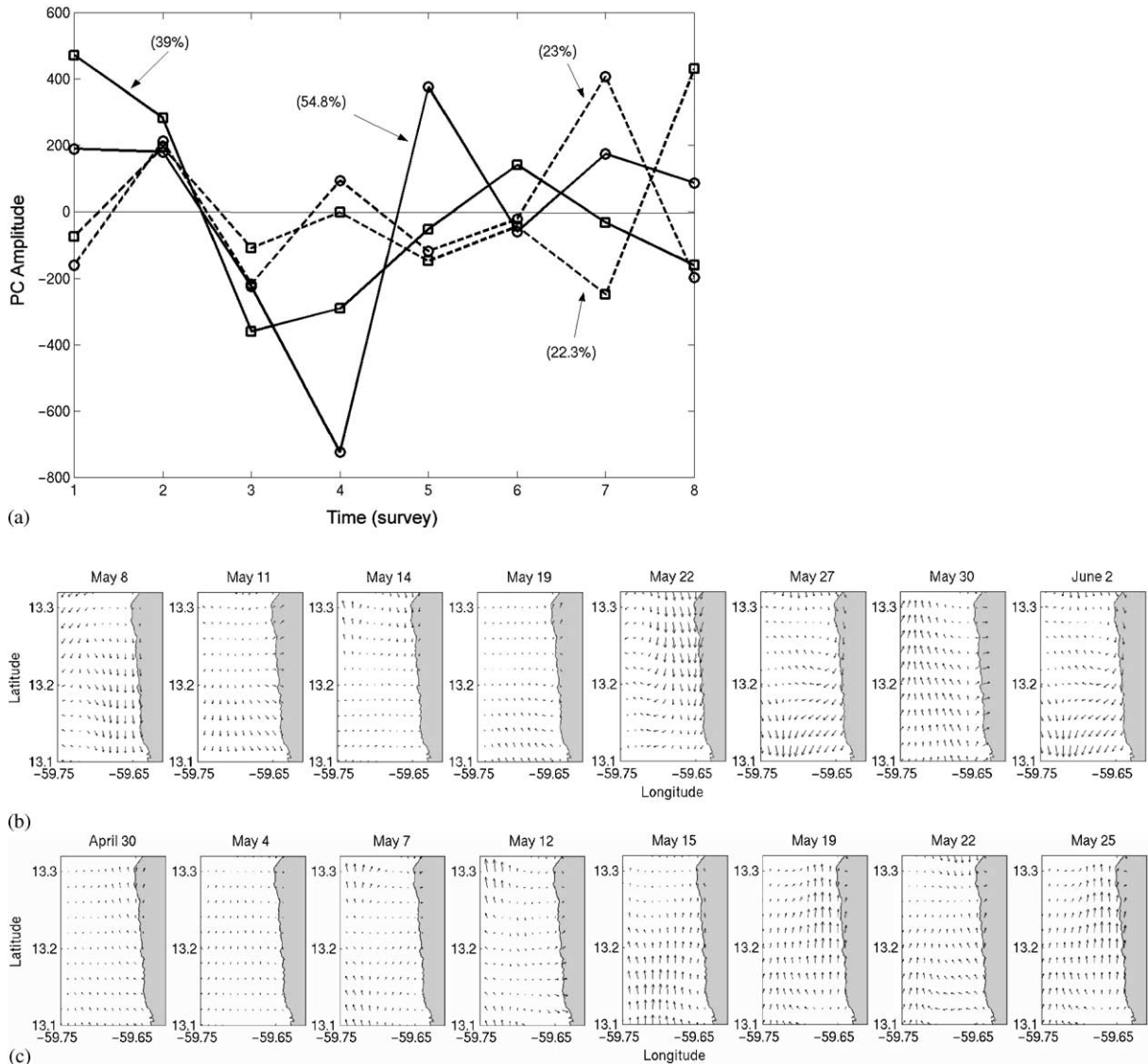


Fig. 10. Temporal distribution of the first (solid lines) and second (dotted lines) PC amplitudes from the velocity field during May 1996 (circle) and 1997 (square) (a); map of the first mode EOF (cm s^{-1}) relative to the eight surveys for 1996 (b) and 1997 (c).

trajectories, although they did not agree well with drifters released right at the surface, where the wind-driven component of the currents may dominate the circulation (Fig. 12); this is not surprising since the ADCP did not measure currents in the upper 10 m of the water column. These results suggest that the flow field derived from MVOA of hydrographic and current data is indeed representative of the near-shore circulation.

Tracking of particles released in the surface layer from the reef showed a maximum residence time of 18 d, indicating the possibility of larval retention within the island-scale circulation. However, there was some inter-annual variation in the retention rates, reflected by differences in mean loss rates during the first 4 d as large as $13.2\% \text{d}^{-1}$ for particles released in May 1996 compared to $4.7\% \text{d}^{-1}$ for those released in May 1997 (Fig. 13).

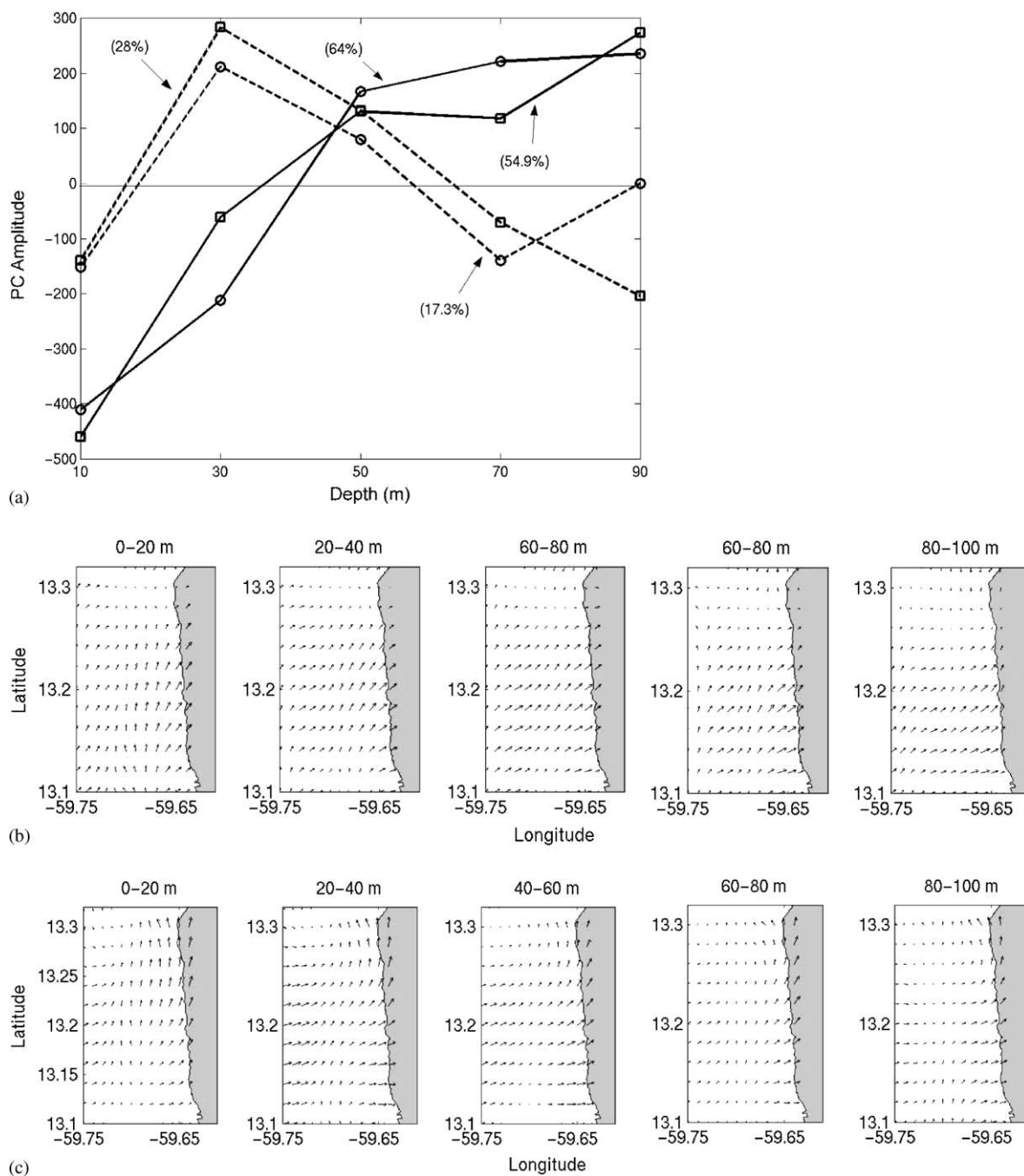


Fig. 11. Vertical distribution of the first (solid lines) and second (dotted lines) PC amplitudes from the velocity field during May 1996 (circle) and 1997 (square) (a); map of the first mode EOF (cm s⁻¹) relative to the 5 layers for 1996 (b) and 1997 (c).

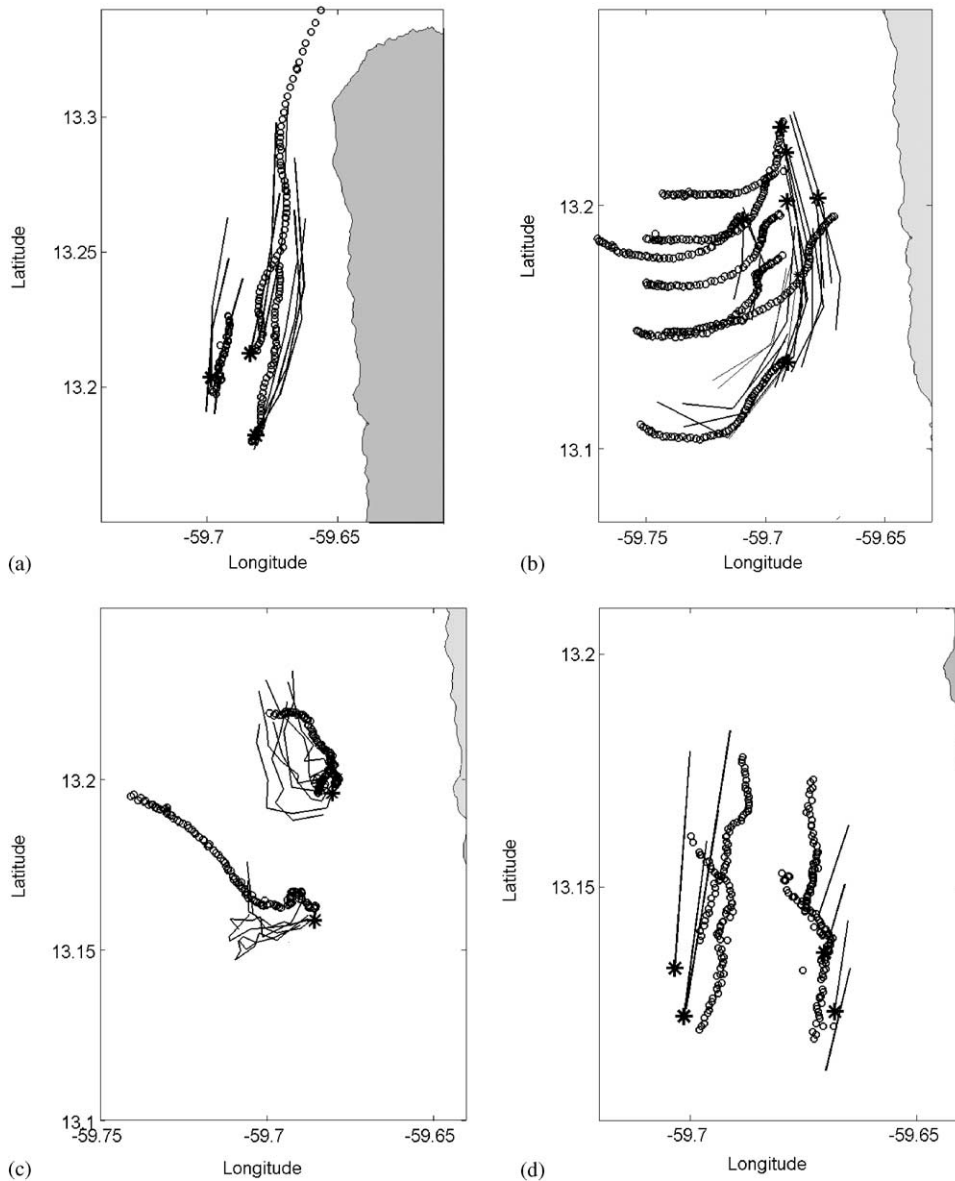


Fig. 12. Comparison of trajectories from real drifters released in the sampling box (circles: 1 circle every 10 min) with those of virtual drifters released in the MVOA flow field (lines: 1 segment every 6 h). Drifters were deployed in 1997 on April 29 at 25 m (a), on May 6 at 2 m (b), on May 9 at 55 m (c), and on May 21 at 40 m (d).

4. Discussion

The coastal environment contains more high frequency variability than does the open ocean environment at similar depths, because of the occurrence of weather systems and tides at time

scales in the range of $0.1\text{--}2\text{ cycles d}^{-1}$ (Brink and Cowles, 1991; Haidvogel et al., 2000). Similarly, the Barbados near-shore environment is characterized by strong temporal variability. The near field of Barbados is subject to large fluctuations in current directions with a periodicity of ca. 20 d,

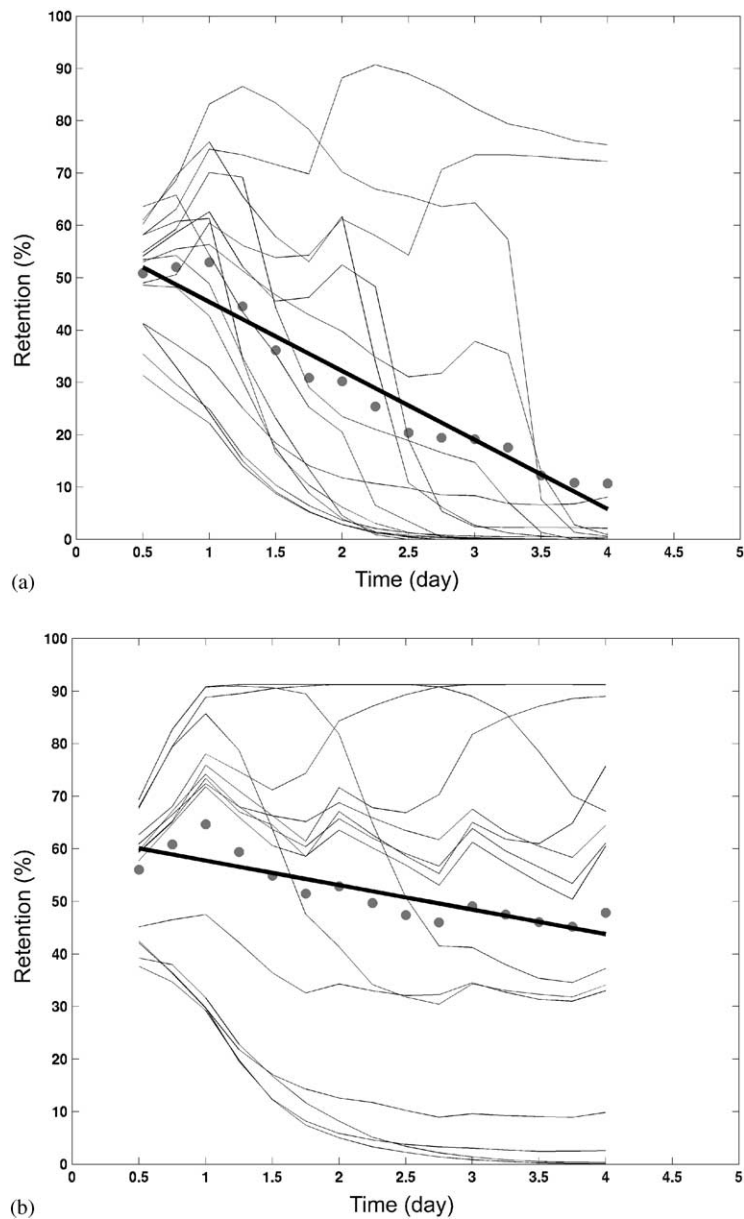


Fig. 13. Comparison of retention rates for particle released along the bank reef on the west coast of Barbados in the surface layer (0–20 m) in 1996 (a) and 1997 (b); the slope of the regression on the mean retention rates (dots) from 15 daily consecutive releases (thin lines, $n = 3000$ for each daily release) indicates the loss rate per day and has a value of -13.4% and -4.7% for 1996 and 1997, respectively.

and salinity fronts interacting with the energetic currents that flow over the steep shelf slope (in Barbados the shelf is almost non-existent and drops quickly to 400 m at a few km from the reef).

Strong incident flows can lead to a significant distortion of the baroclinic flow and may induce disturbances (Gordon and Hugues, 1981). In fact, the observed switch to a barotropic mode in the

upper 100 m during both cruises and the temporal distribution of the PCs indicate clearly that the velocity field is strongly influenced by the dynamics of NBCR approaching the island.

Recent work revealed low-salinity intrusions associated with NBCR in the vicinity of Barbados (Kelly et al., 2000). However, it was not clear whether the low-salinity lenses identified on the west coast of Barbados were remnants of a NBCR interfering with the Barbados ridge, or whether the island intercepted its full structure. The present study shows that when a NBCR entraining low salinity translates towards Barbados, the island first feels the barotropic rim, identified by coherent southward flow (ca. 50 cm s^{-1}). During this period, the assumption of no motion at 200 m is not valid and the geostrophic flow prescribed by dynamic heights alone would misrepresent the circulation, justifying further the choice of MVOA scheme (rejecting the dynamic height when inconsistent with the velocity data). The barotropic motion leads a baroclinic field, with slightly warmer waters and low-salinity signature linked to a strong halocline, which is consistent with trapping low-salinity Amazon waters by the edge of the NBCR core. This organized flow field indicates that the low-salinity intrusions observed repetitively in both years are not remnants of a ring but are its coherent structure impinging on the island of Barbados.

In addition to the direct effect of the NBCR swirl velocities on the flow field, there is evidence that the salinity front interacts with the local circulation and the island bathymetry. Fresh water fluxes are usually one of the major sources of buoyancy, which acts to stratify the water column (Haidvogel et al., 2000). In Barbados, near-shore waters became vertically stratified when low salinity intruded from offshore, providing strong buoyancy flux relative to the small tidal energy available for mixing. The spread of the low-salinity water, in both the vertical and horizontal, is variable and certainly modulated by the NBCR occurrence. When the low-salinity lens is overriding the dense oceanic waters, a stronger baroclinic coastal current is formed. Wind stress usually generates a secondary circulation that can move the buoyant water, by either pushing it

closer to shore or confining it to its offshore origin. This situation can produce upwelling or downwelling circulation associated with along shore currents. Offshore flow at the surface induces upwelling, producing a low horizontal gradient in density but a high vertical one (downwelling produces the opposite). Vertical motion in a limited area is by definition ageostrophic, and, in fact, current reversals coincided with a deepening or a rising of the halocline. In particular, current reversal during survey 5 was coupled with a strong horizontal salinity gradient and the sloping of the associated halocline in the cross-shelf salinity field suggested the presence of downwelling. Vertical motion can be the result of frontogenesis through convergences at distorted fronts, which produce vorticity adjustments and trigger upwelling or downwelling (Wang, 1993; Pinot et al., 1995b). In fact, the map of the first mode EOF in 1997 shows a cyclonic feature in the upper 40 m, which may correspond to an upwelling zone (see Aristegui et al., 1997). Because the MVOA allows the evaluation of the ageostrophic component of the velocity field, irrotational velocities were plotted separately at 10 m (e.g., Fig. 5a) and revealed horizontal variability occurring through convergent and divergent features, a signature of vertical motion. In both years maximum divergence (upwelling) of $0.2 \times 10^{-5} \text{ s}^{-1}$ was found during surveys 7 and 8, and convergence (downwelling) was at its maximum ($-0.15 \times 10^{-5} \text{ s}^{-1}$) during surveys 4, 5, and 6. Although these relative vorticity values are modest, they may generate larger density gradients and induce an ageostrophic circulation (Wang, 1993). Further analysis of the magnitude of the vertical velocity across the salinity front could be investigated with the drifters' data. Downward velocities could represent a significant mechanism for transport and larval retention.

The PCA of velocity relative to the vertical and temporal factors in the study area demonstrates that the analyzed flow field is coherent with depth and time. These results suggest that the space scales and frequency of the sampling, together with the MVOA scheme, reproduce accurately the in situ flow field in the upper 100 m of the water column and can be used for modeling larval

transport. The maximum residence times of water masses in the sampling domain of 8–20 d indicate that locally spawned larvae could be retained in the vicinity of the island during their early stages, and perhaps throughout their larval duration.

5. Conclusions

This study of 3-D circulation in the vicinity of Barbados reveals that external forcing by the NBCR plays a dominant role in the flow field variability. Multivariate OA of high spatio-temporal resolution CTD and ADCP data, together with quantitative PCA, helped in obtaining the detailed flow structure of a dynamic salinity front intercepting the island of Barbados. In both years a NBCR intruded from the south, bringing Amazon waters onto the western shore of the island, and persisting in the domain throughout the rest of the survey. Forcing by the NBCR had a similar effect on the velocity field during both years, within the same temporal and spatial scales. This study constitutes the first evidence that a NBCR can maintain its structure and remain quite coherent as it passes the Tobago–Barbados ridge. Local recruitment variability thus may often result from the influence of those low-salinity events on larval retention and survival, and further, may be predictable. Similarly, when a NBCR continues its course after intercepting Barbados, as indicated by the recent NBCR Experiment (Fleurant et al., 1999; Glikson et al., 2000), it could entrain larvae from Barbados towards the Lesser Antilles and become an agent of population genetic mixing if not significant downstream recruitment (Cowen et al., 2000). This work can be applied to examine larval transport in other island scale flows and help identify the physical parameters affecting the retention and consequent recruitment of coral reef fishes.

Acknowledgements

We would like to thank all who participated in this large endeavor. We are particularly grateful to Su Sponaugle, Mark Sullivan, and Lian-Mei Gao

for discussion and ideas on the manuscript; William Richards, Zulema Garraffo, and Arthur Mariano for helpful reviews; Graham Allen for his help in collecting the physical oceanographic data; Teresa Rotunno, Tom Wilson, Nathalie Reyns, and Brian Steves who gracefully provided technical assistance; Captain Vince Seiler and the Crew on the R.V. *Seward Johnson* who made the long, around-the-clock samplings not only effective but enjoyable. We also thank the reviewers for their constructive comments. This work was funded by the National Science Foundation Grant OCE-9521104.

References

- Aristegui, J., Tett, P., Hernandez-Guerra, A., Basterrere, G., Montero, M.F., Wild, K., Sangra, P., Hernandez-Leon, S., Canton, M., Garcia-Braun, J.A., Pacheco, M., Barton, E.D., 1997. The influence of island-generated eddies on chlorophyll distribution: a study of mesoscale variation around Gran Canaria. *Deep-Sea Research I* 44 (1), 71–96.
- Barton, E.D., Basterretxea, G., Flament, P., Mitchelson-Jacob, E.G., Jones, B., Aristegui, J., Herrera, F., 2000. Lee region of Gran Canaria F. *Journal of Geophysical Research* 105 (C7), 17173–17193.
- Boden, B.P., 1952. Natural conservation of insular plankton. *Nature* 169, 697–699.
- Boehlert, G.W., Watson, W., Sun, L.C., 1992. Horizontal and vertical distributions of larval fishes around an isolated oceanic island in the tropical Pacific. *Deep-Sea Research* 39 (3–4A), 439–466.
- Bowman, M.J., Stansfield, K.L., Fauria, S.J., Wilson, T.C., 1994. Coastal ocean circulation near Barbados, West Indies Spring 1990 and 1991. *Journal of Geophysical Research* 99 (C8), 16131–16142.
- Brink, K.H., Cowles, T.J., 1991. The coastal transition zone program. *Journal of Geophysical Research* 96 (C8), 14637–14647.
- Chiswell, S.M., Booth, J.D., 1999. Rock lobster *Jasus edwardsii* larval retention by the Wairapapa Eddy off New Zealand. *Marine Ecology Progress Series* 183, 227–240.
- Chopra, K.P., 1973. Atmospheric and oceanic flow problems induced by islands. *Advanced Geophysics* 16, 297–421.
- Cowen, R.K., Castro, L.R., 1994. Relation of coral reef fish larvae distributions to island scale distribution around Barbados, West Indies. *Bulletin of Marine Science* 54, 228–244.
- Cowen, R.K., Lwiza, K.M.M., Sponaugle, S., Paris, C.B., Olson, D.B., 2000. Connectivity of marine populations: open or closed? *Science* 287, 857–859.

- Dutkiewicz, S., Griffa, A., Olson, D.B., 1993. Particle diffusion in a meandering jet. *Journal of Geophysical Research* 98 (C9), 16487–16500.
- Flagg, C.N., Gordon, R.L., McDowell, S., 1986. Hydrographic and current observations on the continental slope and shelf of the western equatorial Atlantic. *Journal of Physical Oceanography* 16, 1412–1429.
- Fleurant, C., Wilson, D., Johns, W., Garzoli, S., Smith, R., 1999. CTD/O2, LADCP and XBT Measurements Collected aboard the R/V SEWARD JOHNSON, November–December 1998: North Brazil Current Rings Experiment Cruise 1(NBC-1), NOAA/DROARAOML35; PB2000102446, 268p.
- Fratantoni, D.M., Johns, W.E., Townsend, T.L., 1995. Rings of the North Brazil current: their structure and behavior inferred from observations and a numerical simulation. *Journal of Geophysical Research* 100, 10633–10654.
- Glikson, D.A., Fratantoni, D.M., Wooding, C.M., Richardson, P.L., 2000. North Brazil Current ring experiment: surface drifter data report November 1998–June 2000. Technical Report, July 2000, WHOI-2000-10, 121p.
- Gomis, D., Ruiz, S., Pedder, M.A., 2001. Diagnostic analysis of the 3D ageostrophic circulation from a multivariate spatial interpolation of CTD and ADCP data. *Deep Sea Research Part I* 48 (1), 269–295.
- Goni, G., Johns, W.E., 2001. A census of North Brazil Current Rings observed from TOPEX/POSEIDON altimetry: 1992–1998. *Geophysical Research Letters* 28 (1), 1–4.
- Gordon, H.B., Hugues, R.L., 1981. A study of rotating baroclinic nonlinear flow around an island. *Journal of Physical Oceanography* 11, 1011–1014.
- Haidvogel, D.B., Blanton, J., Kindle, J.C., Lynch, D.R., 2000. Coastal ocean modeling: processes and real-time systems. *Oceanography* 13 (1), 35–46.
- Hogg, N.G., 1972. Steady flow past an island with application to Bermuda. *Geophysical and Astrophysical Fluid Dynamics* 4, 55–81.
- Hogg, N.G., 1980. Effects of bottom topography on ocean currents. In: Hide, R., White, P.W. (Eds.), *Oceanographic Effects in Planetary Flows*, GARP Pub. Ser. 23. World Meteorological Organization, Geneva, pp. 659–682.
- Hogg, N.G., Katz, E.J., Sanford, T.B., 1978. Eddies, islands and mixing. *Journal of Geophysical Research* 83, 2921–2938.
- Johns, W.E., Lee, T.N., Scott, F.A., Zantopp, R.J., Evans, R.H., 1990. The North Brazil Current retroflexion: seasonal structure and eddy variability. *Journal of Geophysical Research* 95, 103–122.
- Kelly, P.S., Lwiza, K.M.M., Cowen, R.K., 2000. Low-salinity pools at Barbados, West Indies: their origin, frequency, and variability. *Journal of Geophysical Research–Oceans* 105 (C8), 19699–19708.
- Larson, M., Hanson, H., Kraus, N.C., Newe, J., 1999. Short- and long-term responses of beach fills determined by EOF analysis. *Journal of Waterway Port Coastal and Ocean Engineering* 125 (6), 733–950.
- Liu, Z.Y., Wu, L.X., Hurlburt, H., 1999. Rossby wave-coastal Kelvin wave interaction in the extratropics. Part II: formation of island circulation. *Journal of Physical Oceanography* 29 (9), 2405–2418.
- Mariano, A.J., Hitchcock, G.L., Ashjian, C.J., Olson, D.B., Rossby, T., Ryan, E., Smith, S.L., 1996. Principal component analysis of biological and physical variability in a Gulf Stream meander crest. *Deep-Sea Research I* 43 (9), 1531–1535.
- Okubo, A., 1971. Oceanic diffusion diagrams. *Deep-Sea Research* 18, 789–802.
- Okubo, A., 1994. The role of diffusion and related physical processes in dispersal and recruitment of marine populations. In: Sammarco, P.W., Heron, M.L. (Eds.), *The Biophysics of Marine Larval Dispersal*. American Geophysical Union, Washington, DC, pp. 5–32.
- Pedder, M.A., 1989. Limited area in kinematic analysis by multivariate statistical interpolation method. *Monthly Weather Review* 117, 1695–1708.
- Pedder, M., Gomis, D., 1998. Application of EOF analysis to the spatial estimation of circulation features in the ocean sampled by high-resolution CTD soundings. *Journal of Atmospheric and Ocean Technology* 15, 959–978.
- Pinot, J.M., Tintore, J., Gomis, D., 1995a. Multivariate analysis of the surface circulation in the Balearic Sea. *Progress in Oceanography* 36, 343–376.
- Pinot, J.M., Tintore, J., Lopez-Jurado, J.L., Fernandez De Puelles, M.L., Jansa, J., 1995b. Three-dimensional circulation of a mesoscale eddy/front system and its biological implications. *Oceanologica Acta* 18 (4), 389–400.
- Polovina, J.J., Kleiber, P., Kobayashi, D.R., 1999. Application of TOPEX-POSEIDON satellite altimetry to simulate transport dynamics of larvae of spiny lobster, *Panulirus marginatus*, in the Northwestern Hawaiian Islands, 1993–1996. *Fishery Bulletin* US 97 (1), 132–143.
- Pond, S., Picard, G.L., 1983. In: Pond, S., Picard, G.L. (Eds.), *Introductory Dynamical Oceanography*. Pergamon Press, Oxford, 329p.
- Richards, W.J., 1982. Planktonic processes affecting establishment and maintenance of reef fish stocks. In: Huntsman, G.R., Nicholson, W.R., Fox, Jr., W.W. (Eds.), *The Biological Bases for Reef Fishery Management*, pp. 92–100. Proceedings of a workshop held October 7–10, 1980 at St. Thomas, Virgin Islands of the United States. NOAA Technical Memorandum NMFS-SEFC-80, 229p.
- Richardson, P.L., Hufford, G.E., Limeburner, R., Brown, W.S., 1994. North Brazil Current retroflexion eddies. *Journal of Geophysical Research* 99, 5081–5094.
- Rosenfeld, L.K., Molinari, R.L., Leaman, K.D., 1989. Observed and modeled annual cycle of transport in the Straits of Florida and east of Abaco Island, the Bahamas (26.5 degree N). *Journal of Geophysical Research* 94 (C4), 4867–4878.

- Sanders, F., 1981. A preliminary assessment of the main causative mechanisms of the “island mass” effect of Barbados. *Marine Biology* 64, 199–205.
- Simmons, H.L., Nof, D., 2000. Islands as eddy splitters. *Journal of Marine Research* 58, 919–956.
- Smith, P.C., Schwing, F.B., 1991. Mean circulation and variability of the eastern Canadian continental-shelf. *Continental Shelf Research* 11 (8–10), 977–1012.
- Sokal, R.R., Rohlf, F.J., 1995. *Biometry: the principles and practice of statistics in biological research*. Freeman, New York, 887p.
- Stansfield, K.L., Bowman, M.J., Fauria, S.J., Wilson, T.C., 1995. Water mass and coastal current variability near Barbados, West Indies. *Journal of Geophysical Research—Oceans* 100 (C12), 24819–24830.
- Thompson, D.J., 1986. A random walk model of dispersion in turbulent flow and its application to dispersion in a valley. *Quarterly Journal of the Royal Meteorological Society* 112, 511–530.
- Wang, D.P., 1993. Model of frontogenesis: subduction and upwelling. *Journal of Marine Research* 51, 497–513.